

**Monitoring AMOC  
with GRACE**

K. Bentel et al.

# Monitoring Atlantic overturning circulation variability with GRACE-type ocean bottom pressure observations – a sensitivity study

**K. Bentel, F. W. Landerer, and C. Boening**

Jet Propulsion Laboratory, California Institute of Technology, 4800 Oak Grove Dr, Pasadena, CA 91109, USA

Received: 1 July 2015 – Accepted: 20 July 2015 – Published: 14 August 2015

Correspondence to: K. Bentel (katrin.i.bentel@jpl.nasa.gov)

Published by Copernicus Publications on behalf of the European Geosciences Union.

Title Page

Abstract

Introduction

Conclusions

References

Tables

Figures



Back

Close

Full Screen / Esc

Printer-friendly Version

Interactive Discussion



## Abstract

The Atlantic Meridional Overturning Circulation (AMOC) is a key mechanism for large-scale northward heat transport and thus plays an important role for global climate. Relatively warm water is transported northward in the upper layers of the North Atlantic Ocean, and after cooling at subpolar latitudes, sinks down and is transported back south in the deeper limb of the AMOC. The utility of in-situ ocean bottom pressure (OBP) observations to infer AMOC changes at single latitudes has been characterized in recent literature using output from ocean models. We extend the analysis and examine the utility of space-based observations of time-variable gravity and the inversion for ocean bottom pressure to monitor AMOC changes and variability between 20 and 60° N. Consistent with previous results, we find a strong correlation between the AMOC signal and OBP variations, mainly along the western slope of the Atlantic basin. We then use synthetic OBP data – smoothed and filtered to resemble the resolution of the GRACE gravity mission – and reconstruct geostrophic AMOC transport. Due to the coarse resolution of GRACE-like OBP fields, we find that leakage of signal across the steep slopes of the ocean basin is a significant challenge at certain latitudes. However, overall, the inter-annual AMOC anomaly time series can be recovered from 20 years of monthly GRACE-like OBP fields with errors less than 1 Sverdrup.

## 1 Introduction

Changes of the Atlantic Meridional Overturning Circulation (AMOC) and associated pole-ward ocean heat transport from the equatorial regions influence climate at higher latitudes significantly, with potentially significant impacts in particular for the Northern Hemisphere as well as Northwest Europe's climate (Manabe and Stouffer, 1999; Srokosz et al., 2012; IPCC, 2014). The dynamics of the mean and time-variable North Atlantic MOC have been described in several recent studies, using observations from hydrographic arrays such as RAPID-MOCHA (e.g., Kanzow et al., 2010; Elipot et al.,

OSD

12, 1765–1791, 2015

## Monitoring AMOC with GRACE

K. Bentel et al.

Title Page

Abstract

Introduction

Conclusions

References

Tables

Figures



Back

Close

Full Screen / Esc

Printer-friendly Version

Interactive Discussion



2013) and MOVE (Send et al., 2011) as well as model studies (e.g., Vellinga and Wood, 2002; Bingham and Hughes, 2008, 2009a; McCarthy et al., 2012; Wunsch and Heimbach, 2013).

AMOC variability manifests itself in ocean bottom pressure (OBP) changes, in particular along the western boundary (e.g., Roussenov et al., 2008; Bingham and Hughes, 2008, 2012), but also in sea surface height changes (e.g., Bingham and Hughes, 2009b) and in sea surface temperatures (Knight et al., 2005; Zhang, 2008). The viability of using OBP along the Eastern and Western boundaries to calculate the basin-wide meridional geostrophic transports was first demonstrated with numerical ocean simulations (e.g., Bingham and Hughes, 2008, 2009a). More recently, Elipot et al. (2013) used bottom pressure recorder (BPR) measurements along the Western boundary to monitor AMOC. However, due to the inherent drift problems of in-situ BPR recorders, their analysis was limited to time scales shorter than one year, as well as to the zonal cross section of instrument deployment.

In the present study, we build upon previous results (i.e., Roussenov et al., 2008; Bingham and Hughes, 2008, 2009a) and examine the feasibility of using OBP to derive AMOC variations. While the previous works examined the relationships between OBP and AMOC variability in the North Atlantic at specific latitudes (e.g., 40, 48 and 50° N), we examine the entire latitude and depth range from 20 through 60° N. Specifically, we investigate the detectability of AMOC variability using OBP inferred from time-variable gravity observations such as those provided by the GRACE satellites (Tapley et al., 2004). The GRACE gravity observations provide complete global spatial coverage and monthly time series of ocean mass changes from 2002 until present (Chambers and Bonin, 2012). The challenge in using GRACE-OBP to derive AMOC variability is the relatively coarse spatial resolution as well as overall signal-to-noise levels. To estimate the effects of limited spatial resolution, we employ data from the ECCO2 ocean state estimate and convert the synthetic OBP fields to a GRACE-like resolution. To also capture signal contamination from nearby land hydrology variations (which are also recorded by GRACE), we evaluate the effects of terrestrial land water storage on GRACE-like

## Monitoring AMOC with GRACE

K. Bentel et al.

Title Page

Abstract

Introduction

Conclusions

References

Tables

Figures



Back

Close

Full Screen / Esc

Printer-friendly Version

Interactive Discussion



## Monitoring AMOC with GRACE

K. Bentel et al.

Title Page

Abstract

Introduction

Conclusions

References

Tables

Figures

◀

▶

◀

▶

Back

Close

Full Screen / Esc

Printer-friendly Version

Interactive Discussion



OBP retrievals by combining the ocean state estimate with a land-hydrology model. Our results indicate that even though resolution along the steep basin slopes is challenging in GRACE-like OBP fields, we find that the recovery of the meridional volume transports with errors less than 1 Sv is possible for specific regions and time scales.

Our paper is organized as follows: in Sect. 2, we briefly review the pertinent aspects of the underlying theories and relationships between OBP and AMOC transports; then we describe the ocean state estimate ECCO2 and discuss the AMOC and OBP signals in the model at GRACE-like spatial resolution, including signal contamination effects from land hydrology; in Sect. 3 we present results for deriving AMOC from the model data directly compared to results for AMOC from data smoothed to a GRACE-like resolution.

## 2 Methods and data

### 2.1 Theoretical background

The Atlantic meridional overturning circulation consists of a northward flow in the upper layer of the ocean (mostly between the surface and 1000 m depth; Srokosz et al., 2012; Wunsch and Heimbach, 2013), and a return flow to the south in the deeper layer of the ocean (between approximately 1000 and 5000 m depth). The meridional stream function  $\psi(y, x)$  is derived from meridional velocities ( $v_y$ ) by integration over longitudes ( $x$ ) and depths ( $z$ ) (Marotzke et al., 1999),

$$\psi(y, z) = \int_E^W \int_{\eta}^z v_y dz dx. \quad (1)$$

As the large-scale flows are dominated by a geostrophic balance, the meridional transport  $T(z)$ , at a particular latitude ( $y$ ) and depth ( $z$ ), can be derived from the zonal

bottom pressure differences  $p_E$  and  $p_W$  at the eastern and western basin boundaries by taking

$$T(z) = \frac{p_E(z) - p_W(z)}{\rho_0 f}, \quad (2)$$

where the constants are the Coriolis parameter  $f$  and the mean sea water density  $\rho_0$  (Marotzke et al., 1999; Roussenov et al., 2008). Acceleration and stress terms are neglected, as they only play a role in the Ekman layer and in the deep bottom layers. For a more rigorous derivation and justification for Eq. (2) we defer to Bingham and Hughes (2008, 2009a), and Roussenov et al. (2008), and references therein. Using the geostrophic approximation, the depth-integrated meridional transports  $T(z)$  at a particular latitude ( $y$ ) can then be used to give the meridional stream function  $\psi$  at that latitude:

$$\psi(y, \Delta z) = \frac{1}{\rho_0 f} \int_{z_1}^{z_2} (p_E - p_W) dz. \quad (3)$$

Equation (3) provides a method to derive the geostrophic component of the AMOC stream function (or volume transport between two layers) from ocean bottom pressure data along the boundaries of the ocean basin. Possibly intervening topography (i.e., mid-ocean ridges) should in theory be considered when evaluating Eq. (3), but Bingham and Hughes (2008) and Bingham and Hughes (2009a) demonstrated in an ocean model that for inter-annual time-variable transports (periods greater than annual) in the North Atlantic, bottom pressure variability is concentrated along the Western boundary, and it is sufficient to use only the outermost Eastern and Western points across the basin section (if a basin-mean or depth averaged boundary pressure is removed from  $p_W$  in Eq. (3), it is also possible to use only bottom pressure on the Western boundary (Bingham and Hughes, 2009a). Furthermore, the dominance of the Western boundary variations was recently confirmed from hydrographic in-situ data (Elipot et al., 2013).

Monitoring AMOC  
with GRACE

K. Bentel et al.

Title Page

Abstract

Introduction

Conclusions

References

Tables

Figures

◀

▶

◀

▶

Back

Close

Full Screen / Esc

Printer-friendly Version

Interactive Discussion



**Monitoring AMOC  
with GRACE**

K. Bentel et al.

Title Page

Abstract

Introduction

Conclusions

References

Tables

Figures



Back

Close

Full Screen / Esc

Printer-friendly Version

Interactive Discussion



We reconfirmed this with the ocean model ECCO2 (see below for details), and thus use  $\rho_E$  and  $\rho_W$  only for our analyses in the North Atlantic. While knowledge of  $\rho_E$  and  $\rho_W$  along the boundaries is in principle sufficient to infer  $\psi(y, z)$ , the actual measurement of these terms is challenging. In-situ BPRs suffer from notorious drift-problems, and thus require drift corrections that usually inhibit any inferences about longer-than-annual variations (Polster et al., 2009). An alternative measurement of OBP variations can be obtained from time-variable gravity observations from space as currently acquired by the GRACE satellites (e.g., Tapley et al., 2004). The main challenge for OBP inferred from time-variable gravity is the limited horizontal resolution, as well as the required signal sensitivity. Due to the altitude (about 450 km) and orbit configuration of the two GRACE satellites, the horizontal spatial resolution is limited to approximately 300 km (e.g., Chambers and Bonin, 2012; Landerer and Swenson, 2012). Much of the AMOC-related OBP signals occur along the narrow and steep Western boundary slope and are thus difficult to resolve. In Sect. 3, we therefore quantify these resolution issues using synthetic data at GRACE-like spatial resolutions to quantify the feasibility of the OBP-AMOC approach. Also note that GRACE can only resolve OBP variations relative to a (arbitrary) time-mean. Therefore, all terms in Eqs. (1)–(3) are taken to be anomalies and therefore only AMOC variations can be inferred, but not its long-term average. The mean flow in the North Atlantic and the resulting OBP anomalies are illustrated in Fig. 1.

## 2.2 Synthetic OBP observations

We use the Estimating the Circulation and Climate of the Ocean, Phase II (ECCO2, Menemenlis et al., 2008) to reconstruct the AMOC variability from simulated OBP observations in the North Atlantic as in Eq. (3). The OBP-derived AMOC reconstructions are compared against the model baseline AMOC, which represents the model truth and is based on the meridional velocities according to Eq. (1). Similar to Bingham and Hughes (2008), we extract zonal OBP profiles following the model's bathymetry, and then interpolate these values to regularly spaced 100 m depth intervals. Monthly

ECCO2-OBP data at a horizontal resolution of  $0.25^\circ$  is computed for the time period January 1993 through December 2012, for the area of the North Atlantic,  $80-0^\circ$  W longitude and  $20-60^\circ$  N latitude. We remove a global mean OBP term to enforce mass conservation (Greatbatch, 1994). For the subsequent analysis, we removed a trend and the mean annual climatology signal from all time series (OBP, velocities), and smooth with a 15-month running mean to focus on inter-annual signals only.

### 2.3 GRACE-like OBP fields: mascons and spherical harmonics

We evaluate OBP output from the ECCO2 ocean state estimate as provided at a  $0.25^\circ$  degree resolution. To create GRACE-like synthetic observations that match actual GRACE resolution, we smooth the OBP fields to a  $3^\circ$  equal area grid. This grid is identical to the JPL-mascon RL05M grid (Watkins et al., 2015). Second, the OBP data is smoothed to resemble the resolution of the standard GRACE solutions, which are represented in spherical harmonics truncated at degree and order 60, and smoothed with a Gaussian filter with 300 km radius to reduce noise and correlated errors that are present in real GRACE data. This processing provides approximately the resolution that is currently achieved with the GRACE satellites. However, we do not consider instrument and resulting measurement errors in the gravity field retrieval from GRACE measurements in order to focus on the issues of spatial resolution and signal leakage. The spatial smoothing and averaging of the  $0.25^\circ$  OBP fields leads to significant resolution reduction in particular in highly energetic regions like the Gulf stream, as well as in regions of steep bathymetry (Figs. 2 and 3).

### 2.4 Leakage effects

#### 2.4.1 From continental hydrology

In order to make the synthetic OBP observations more realistic, we add a continental hydrology signal that we obtain from the GLDAS-NOAH hydrology model (Rodell

Title Page

Abstract

Introduction

Conclusions

References

Tables

Figures



Back

Close

Full Screen / Esc

Printer-friendly Version

Interactive Discussion



## Monitoring AMOC with GRACE

K. Bentel et al.

Title Page

Abstract

Introduction

Conclusions

References

Tables

Figures

◀

▶

◀

▶

Back

Close

Full Screen / Esc

Printer-friendly Version

Interactive Discussion



et al., 2004). The continental hydrology signal does not affect the OBP data on the 0.25° ECCO2 grid. However, when the data is smoothed, the hydrology signal “leaks” into the OBP data (Wahr et al., 1998; Chambers and Bonin, 2012), causing aliasing of land hydrology variations on ocean grid points (Fig. 4). As the following analysis will show, the effects of land signal leakage tend to dominate the error budget in the meridional transport and overturning calculations, in particular for the near-coastal shallower shelf areas (above approx. 1000 m). Therefore, a leakage correction (e.g., CRI filter for the mascon-grid) is essential in order to employ GRACE OBP-observations: mascons that cover both land and ocean area still obtain only one value to represent the mass change within that mascon. To better distinguish where the signals originate from, a so-called coastline resolution improvement (CRI) filter is employed (see Watkins et al., 2015, for details). Essentially, the CRI process separates land hydrology and ocean signals based on a-priori co-variance information from both land and ocean forward simulations. This CRI filter reduces the leakage of the continental hydrology signal into the adjacent ocean mascons significantly (Fig. 4).

### 2.4.2 Due to steep bathymetry gradients

Not only signal leakage from continental hydrology has to be taken into account in GRACE-like resolutions, but also leakage of signal within the ocean, over different depths. Especially along the steep basin boundary slopes, there are instances where one 3° mascon covers a number of different depth layers. Thus, the different OBP in these layers cannot be resolved. One possibility to make this leakage effect smaller is optimal placement in longitude of the individual mascon cells. In the JPL mascon grid, it is possible to shift the mascons in longitude direction (for each mascon latitude) without influencing mascons in other latitudes. We create a synthetic data set where we position the JPL mascons optimal to resolve as much of the Western and Eastern boundary signal as possible.

### 3 Results

Equation 3 is evaluated for different synthetic OBP resolutions derived from ECCO2 in the North Atlantic: the original ECCO2 0.25° grid ( $T^O$ ), a GRACE spherical harmonics grid truncated at 60° ( $T^{SH60}$ ), GRACE mascon grids, without ( $T^{MSC}$ ) and with ( $T^{MSC+CRI}$ ) CRI filter, and position optimized mascons ( $T^{MSC+POSOPT}$ ). See Table 1 for a summary of the corresponding OBP grid characteristics. The OBP-reconstructed transports are then evaluated against the model baseline transports, which are derived directly from the forward-simulated meridional velocities. While the OBP signal on the Western basin boundary contains most of the AMOC information, a basin mode has to be taken into account, either by differencing with the signal on the Eastern boundary, or by removing a depth-averaged OBP to remove variations not contributing to geostrophic transports (Bingham and Hughes, 2008, 2009a). Even though the Eastern boundary OBP contributes only a small fraction to the AMOC signal, we take the signal on the Eastern boundary into account rather than removing a depth-mean. By removing a mean over all depths, leakage signal from continental hydrology would contaminate the OBP data at greater depths as well as the shallower areas, and degrade the AMOC transport estimates compared to the East-West difference. Thus, we consider the Eastern boundary in our calculation, even though the data on the Eastern boundary reduces the signal-to-noise ratio.

#### 3.1 Meridional transports from OBP integration

For each of the synthetic OBP data sets, meridional transport time series are computed in 1° latitude increments and over 100 m depth intervals, and the RMS differences between reconstructed and model reference time series are computed for each depth and latitude and shown in Fig. 5. The results for OBP without a hydrology signal (Fig. 5, top row) at the 0.25° native ECCO2 resolution leads to errors smaller than 0.5 Sv km<sup>-1</sup> for depths between 1000 and 5000 m. At latitudes lower than 50° N, errors above 1000 and below 5000 m vary with latitude and depend on the bathymetry gra-

Title Page

Abstract

Introduction

Conclusions

References

Tables

Figures



Back

Close

Full Screen / Esc

Printer-friendly Version

Interactive Discussion



## Monitoring AMOC with GRACE

K. Bentel et al.

Title Page

Abstract

Introduction

Conclusions

References

Tables

Figures



Back

Close

Full Screen / Esc

Printer-friendly Version

Interactive Discussion



dients. At GRACE-like resolutions (Fig. 5b and c), the errors are slightly higher across all depths, and at specific latitudes, e.g., at 25° N, there are significant signal leakage errors that introduce significant transport retrieval errors. In all the three figures, very high errors ( $> 1.5 \text{ Sv km}^{-1}$ ) occur in the upper 100 m depth for all latitudes. They are due to the non-geostrophic, wind-driven transport in the Ekman layer, which cannot be recovered from East-West OBP difference observations. In all following computations of the geostrophic volume transports, we therefore exclude the upper 100 m. While the GLDAS hydrology signal does not affect the results on the ECCO2 model grid (Fig. 5d), significant leakage errors from land hydrology are introduced when the OBP and hydrology signals are spatially smoothed to GRACE-like resolutions (Fig. 5e and f). Without hydrology leakage, errors of  $1.5 \text{ Sv km}^{-1}$  and larger only occur in the uppermost 100 m when Ekman transports are not accounted for, and at 25° N for the mascons. With hydrology leakage effects, the GRACE-like OBP resolutions lead to high errors that extend into deeper layers, down to 3000–5000 m depth for latitudes 32–40° N. This effect is highly latitude-dependent, since the lower resolution only degrades the results if smoothing occurs over too many depth layers and/or the coastline. In this way, the results are very dependent on the bathymetry and the proximity of depth contours to land points, as well as signal amplitudes over land. In addition, pressure variations over steep bathymetry cannot be adequately resolved in the spatially smoothed data. For the mascon resolution, the leakage effect changes with mascon latitudes. Significant hydrology signal leakage occurs especially between 35 and 40° N, down to a depth of 2000 m. For spherical harmonics, the leakage effects are more smeared out over depths and latitudes. Between 20 and 40° N down to 3000 m depth errors are between 1 and  $2 \text{ Sv km}^{-1}$ . For the mascon results, the CRI filter reduces much of the leakage artefacts; the major leakage effect between 35 and 40° N is reduced from errors exceeding  $2 \text{ Sv km}^{-1}$  to less than  $1 \text{ Sv km}^{-1}$  by 2000 m depth. Another strategy to reduce leakage is to optimize the placement of the individual mascons in longitude direction (for each mascon latitude). When mascon boundaries align with the coastline, hydrology leakage is reduced, and when an individual mascon does not cover too many

depth layers, leakage between depths in the ocean is reduced. The optimal mascon position (in longitude) is found by minimizing both types of errors simultaneously. While there are latitudes, where land leakage is not reduced as much by optimal positioning as by the CRI filter (e.g., 22° N, 33° N), errors in the deeper layers between 2000 and 3000 m depths are smaller than for the CRI results. For 30–50° N and between 1500 and 5000 m depth most errors are below 0.5 Sv km<sup>-1</sup> with the position optimized mascons, while they tend to be between 0.5 and 1 Sv km<sup>-1</sup> in the results with CRI. Note that CRI only treats and reduces land-leakage, but does not mitigate leakage between different ocean depths layers (Watkins et al., 2015).

### 3.2 Reconstructing north- and southward transports

The maximum of the mean model AMOC in ECCO2 lies at 32° N and 909 m depth, Fig. 6. Thus, net transports from the surface to 909 m are northward, and net transports below 909 m to a depth of about 5000 m southward. The circulation below about 5000 m is linked to the Atlantic Bottom Water and is not considered in the following. As mentioned before, the uppermost 100 m of the ocean are also excluded, because the Ekman circulation and related transports cannot be recovered from OBP gradients. Over inter-annual periods, the net water volume transported northward should equal the water volume transported back south (e.g., Srokosz et al., 2012). Thus, it should be sufficient to observe either the northward or the southward transport in order to reconstruct the inter-annual AMOC transport variations.

In what follows, three different depth layers are considered in more detail: 100–909, 909–3000, and 3000–5000 m depth, and detectability of the AMOC signal in each of these three layers from GRACE-like OBP resolutions is assessed. The first layer covers the northward transport (down to the maximum of the mean AMOC, Fig. 6), the second layer covers steep ocean basin slopes for most latitudes (Fig. 2), and the third layers covers deeper transport, where the bathymetry is less steep (Fig. 2), and therefore can be expected to be more favorable for GRACE-like resolutions.

Title Page

Abstract

Introduction

Conclusions

References

Tables

Figures



Back

Close

Full Screen / Esc

Printer-friendly Version

Interactive Discussion



## Monitoring AMOC with GRACE

K. Bentel et al.

Title Page

Abstract

Introduction

Conclusions

References

Tables

Figures



Back

Close

Full Screen / Esc

Printer-friendly Version

Interactive Discussion



Figure 7 shows RMS errors and correlation coefficients for the reconstructed transport versus the model baseline for the three layers. The reconstructed transport from OBP at the ECCO2 native  $0.25^\circ$  resolution (red curves Fig. 7) matches the model baseline transport best; it shows smallest RMS errors (about 0.5 Sv and below, with a maximum of 1 Sv) for all the three layers and the highest correlation coefficients. The average error RMS and correlation level is similar for all the three layers under consideration. However, when smoothing to GRACE-like resolutions, RMS differences become larger and correlation coefficients smaller, due to the much coarser resolution of  $3^\circ$  (yellow, green, blue and black curves in Fig. 7). For these resolutions, overall and maximum RMS errors (Fig. 7) are larger for the medium depth layer (909–3000 m) than for the upper and the deep layers. The larger errors between  $20$  and  $45^\circ$  N in the medium layer for data at GRACE-like resolutions are caused by the steep slopes between about 2000 and 4000 m depth (Figs. 2 and 4). When the data is smoothed, the OBP values cannot be attributed to the correct depth as the depth interval for one  $3^\circ$  smoothing interval becomes very large. Between  $45$  and  $60^\circ$  N, the depth gradient for a  $3^\circ$  longitude interval becomes much smaller, i.e., more than one three degree pixel is needed to cover the depth gradient from 909 to 3000 m. Thus, OBP at depth can be better resolved and the transport reconstruction is more accurate, leading to smaller error RMS. For the upper transport, RMS errors are high (0.5–2 Sv) for spherical harmonics, mascons, and position optimized mascons (yellow, green, and black curves in Fig. 7), and especially high between  $30$  and  $40^\circ$  N. These errors are attributed to leakage effects from land hydrology signals (Fig. 5). In the upper layer, the coastline resolution improvement correction makes a big difference: For mascons with CRI (blue curve in Fig. 7) the error RMS are at a level similar to the ECCO2 native  $0.25^\circ$  resolution and below 1 Sv. In the deep layer (3000–5000 m depth), there are still high error RMS of about 3 Sv between  $30$  and  $40^\circ$  N for spherical harmonics and mascons, because land hydrology leakage extends to depths below 3000 m for these latitudes (Fig. 5). The CRI algorithm and position optimizing of mascons corrects for these errors, therefore, error RMS for mascons with CRI and position optimized mascons are about and below 1 Sv

in the deep layer for 20–45° N. Beyond 45° N, the GRACE resolution is well capable to capture all the OBP signal, since the bathymetry is less steep. Therefore, error RMS decrease, and drop below 0.5 Sv for 50–60° N.

Correlation coefficients vary a lot with latitude. While correlation coefficients are highest for the 0.25° ECCO2 resolution, the difference to the GRACE-like resolutions is the largest in the medium layer, due to steep basin boundary in this layer, as explained above. Even though there are a few latitudes with poor correlation in the deep layer for the GRACE-like resolutions (e.g., between 25 and 30° N, and 40 to 50° N), the correlation coefficients are overall higher than in the upper two layers, where most correlation coefficients are below 0.5. Again, this indicates that the less steep bathymetry in the deep layer is more favorable for GRACE-like resolutions.

In conclusion, Fig. 7 shows that the upper and the deep layer transport can be reconstructed from GRACE-like OBP resolutions with error RMS of 0.5 Sv and correlation coefficients of about 0.7, as long as leakage from land hydrology is accounted and corrected for. The medium layer (909–3000 m depth) is much less suitable for transport reconstruction from GRACE-like OBP resolutions, because the steep bathymetry in this layer cannot be resolved well by GRACE.

Finally, Fig. 8 shows reconstructed transport time series at two example latitudes, 30 and 35° N. The quality of the reconstruction is very different for the two example latitudes, illustrating how latitude dependent the reconstruction is, and how much it depends on the bathymetry. At 30° N, there is no difference between mascons and mascons with CRI (green curves are entirely covered by the blue ones, left panel Fig. 8), i.e., the CRI correction does not introduce any changes, while at 35° N the signal without leakage correction shows very high amplitudes, far from the model baseline to be recovered (red dashed line Fig. 8). The same holds for the results from spherical harmonics (yellow curves Fig. 8), since there is no leakage correction, and the spherical harmonics have no spatial localization (in contrast to the mascons), the yellow curves disagree a lot from the model baseline. The reconstructed signal from OBP on the 0.25° ECCO2 model grid matches the model baseline closely at 30° N and in the deep

**Monitoring AMOC  
with GRACE**

K. Bentel et al.

Title Page

Abstract

Introduction

Conclusions

References

Tables

Figures



Back

Close

Full Screen / Esc

Printer-friendly Version

Interactive Discussion



**Monitoring AMOC  
with GRACE**

K. Bentel et al.

Title Page

Abstract

Introduction

Conclusions

References

Tables

Figures

◀

▶

◀

▶

Back

Close

Full Screen / Esc

Printer-friendly Version

Interactive Discussion



layer at 35° N. For 35° N in the upper two layers the model baseline transport cannot even be recovered entirely at model resolution OBP due to interference with the prevailing dynamics in the Strait of Gibraltar that likely breaks up the relationship between bottom pressure gradients and AMOC transport. At 30° N the deep transport (3000–5000 m) reconstruction from mascon resolutions gives equally good results as the native ECCO2 resolution. This is due to the bathymetry, which does not have very steep gradients at this depth and latitude (see Fig. 2) and therefore the AMOC signal can be reconstructed equally well from the lower, GRACE-like, resolutions as from the native 0.25° grid. In contrast, steep bathymetry gradients are problematic for the coarser OBP resolutions and make AMOC recovery very difficult, as at 35° N. The two examples demonstrate that the reconstruction can be rather latitude- and bathymetry-dependent. But they also show that reconstruction of the AMOC signal from GRACE-like OBP data works best in the deep layer, 3000–5000 m, because the bathymetry is less steep there and it is therefore possible to resolve OBP at 100 m depth intervals with the GRACE-like (about 3°) spatial resolution.

#### 4 Summary and outlook

Our model studies have shown that even though signal leakage (from hydrology and across depths) is a challenge at GRACE-like resolutions, the AMOC anomaly time series can be extracted from GRACE-like OBP observations with errors of 1 Sv and below. The AMOC retrieval is rather sensitive to the bathymetry profile, and therefore the quality of the signal recovery is very latitude dependent (Fig. 7, errors vary with latitude and depth layer from 0.05–5 Sv). However, in the deeper layers of the ocean (where the bathymetry gradients are less steep than in shallower layers), OBP measurements at GRACE-like resolutions lead to errors below 1 Sv, while they are up to 3 Sv for the other two layers (Fig. 7). Thus, the deep layer appears to be the most suitable target to retrieve AMOC transports from OBP observations at GRACE-like resolutions.

## Monitoring AMOC with GRACE

K. Bentel et al.

Title Page

Abstract

Introduction

Conclusions

References

Tables

Figures



Back

Close

Full Screen / Esc

Printer-friendly Version

Interactive Discussion



Since the AMOC is not very coherent with latitude and OBP recorder measurements suffer from drift over longer periods of time, satellite gravity measurements (GRACE-like OBP) present a unique dataset to monitor AMOC changes over large areas (like the whole North Atlantic basin) and over extended periods of time (GRACE time series span from 2002 up to today). Our next steps and ongoing work are to move from model simulations to real data and use the OBP integration analysis on JPL5M GRACE mascons to derive real AMOC anomaly time series from the satellite-based OBP observations.

*Acknowledgements.* The research described in this paper was carried out at the Jet Propulsion Laboratory, California Institute of Technology, sponsored by the National Aeronautics and Space Administration (NASA), and with support from the NASA Physical Oceanography program.

The author's copyright for this publication has been transferred to the Californian Institute of Technology. US Government sponsorship acknowledged.

## References

- Bingham, R. J. and Hughes, C. W.: Determining North Atlantic meridional transport variability from pressure on the western boundary: A model investigation, *J. Geophys. Res.*, 113, C09008, doi:10.1029/2007JC004679, 2008. 1767, 1769, 1770, 1773
- Bingham, R. J. and Hughes, C. W.: Geostrophic dynamics of meridional transport variability in the subpolar North Atlantic, *J. Geophys. Res.*, 114, C12029, doi:10.1029/2009JC005492, 2009a. 1767, 1769, 1773
- Bingham, R. J. and Hughes, C. W.: Signature of the Atlantic meridional overturning circulation in sea level along the east coast of North America, *Geophys. Res. Lett.*, 36, L02603, doi:10.1029/2008GL036215, 2009b. 1767
- Bingham, R. J. and Hughes, C. W.: Local diagnostics to estimate density-induced sea level variations over topography and along coastlines, *J. Geophys. Res.*, 117, C01013, doi:10.1029/2011JC007276, 2012. 1767

## Monitoring AMOC with GRACE

K. Bentel et al.

Title Page

Abstract

Introduction

Conclusions

References

Tables

Figures

◀

▶

◀

▶

Back

Close

Full Screen / Esc

Printer-friendly Version

Interactive Discussion



Chambers, D. P. and Bonin, J. A.: Evaluation of Release-05 GRACE time-variable gravity coefficients over the ocean, *Ocean Sci.*, 8, 859–868, doi:10.5194/os-8-859-2012, 2012. 1767, 1770, 1772

Elipot, S., Frajka-Williams, E., Hughes, C. W., and Willis, J. K.: The Observed North Atlantic Meridional Overturning Circulation: Its Meridional Coherence and Ocean Bottom Pressure, *J. Phys. Oceanogr.*, 44, 517–537, doi:10.1175/JPO-D-13-026.1, 2013. 1766, 1767, 1769

Greatbatch, R. J.: A note on the representation of steric sea level in models that conserve volume rather than mass, *J. Geophys. Res.*, 99, 12767–12771, 1994. 1771

IPCC: Climate Change 2014: Impacts, Adaptation, and Vulnerability, Part A: Global and Sectoral Aspects, in: Contribution of Working Group II to the Fifth Assessment Report of the Intergovernmental Panel on Climate Change, edited by: Field, C. B., Barros, V. R., Dokken, D. J., Mach, K. J., and Mastrandrea, M. D., Cambridge University Press, New York, NY, USA, 2014. 1766

Kanzow, T., Cunningham, S. a., Johns, W. E., Hirschi, J. J.-M., Marotzke, J., Baringer, M. O., Meinen, C. S., Chidichimo, M. P., Atkinson, C., Beal, L. M., Bryden, H. L., and Collins, J.: Seasonal Variability of the Atlantic Meridional Overturning Circulation at 26.5° N, *J. Clim.*, 23, 5678–5698, doi:10.1175/2010JCLI3389.1, 2010. 1766

Knight, J. R., Allan, R. J., Folland, C. K., Vellinga, M., and Mann, M. E.: A signature of persistent natural thermohaline circulation cycles in observed climate, *Geophys. Res. Lett.*, 32, L20708, doi:10.1029/2005GL024233, 2005. 1767

Landerer, F. W. and Swenson, S. C.: Accuracy of scaled GRACE terrestrial water storage estimates, *Water Resour. Res.*, 48, W04531, doi:10.1029/2011WR011453, 2012. 1770

Manabe, S. and Stouffer, R. J.: The role of thermohaline circulation in climate, *Tellus B*, 51, 91–109, doi:10.1034/j.1600-0889.1999.00008.x, 1999. 1766

Marotzke, J., Giering, R., Zhang, K. Q., Stammer, D., Hill, C., and Lee, T.: Construction of the adjoint MIT ocean general circulation model and application to Atlantic heat transport sensitivity, *J. Geophys. Res. Ocean.*, 104, 29529–29547, doi:10.1029/1999JC900236, 1999. 1768, 1769

McCarthy, G., Frajka-Williams, E., Johns, W. E., Baringer, M. O., Meinen, C. S., Bryden, H. L., Rayner, D., Duchez, a., Roberts, C., and Cunningham, S. a.: Observed interannual variability of the Atlantic meridional overturning circulation at 26.5° N, *Geophys. Res. Lett.*, 39, L19609, doi:10.1029/2012GL052933, 2012. 1767

**Monitoring AMOC  
with GRACE**

K. Bentel et al.

Title Page

Abstract

Introduction

Conclusions

References

Tables

Figures



Back

Close

Full Screen / Esc

Printer-friendly Version

Interactive Discussion



- Menemenlis, D., Campin, J.-M., Heimbach, P., Hill, C., Lee, T., Nguyen, A., Schodlok, M., and Zhang, H.: ECCO2: High Resolution Global Ocean and Sea Ice Data Synthesis, *Mercat. Ocean Q. Newsl.*, p. 13, 2008. 1770
- Polster, A., Fabian, M., and Villinger, H.: Effective resolution and drift of paroscientific pressure sensors derived from long-term seafloor measurements, *Geochemistry, Geophys. Geosystems*, 10, Q08008, doi:10.1029/2009GC002532, 2009. 1770
- Rodell, M., Houser, P. R., Jambor, U., Gottschalck, J., Mitchell, K., Meng, C.-J., Arsenault, K., Cosgrove, B., Radakovich, J., Bosilovich, M., Entin, J. K., Walker, J. P., Lohmann, D., and Toll, D.: The Global Land Data Assimilation System, *B. Am. Meteorol. Soc.*, 85, 381–394, doi:10.1175/BAMS-85-3-381, 2004. 1771
- Rousenov, V. M., Williams, R. G., Hughes, C. W., and Bingham, R. J.: Boundary wave communication of bottom pressure and overturning changes for the North Atlantic, *J. Geophys. Res.*, 113, C08042, doi:10.1029/2007JC004501, 2008. 1767, 1769
- Send, U., Lankhorst, M., and Kanzow, T.: Observation of decadal change in the Atlantic meridional overturning circulation using 10 years of continuous transport data, *Geophys. Res. Lett.*, 38, 1–5, doi:10.1029/2011GL049801, 2011. 1767
- Srokosz, M., Baringer, M., Bryden, H., Cunningham, S., Delworth, T., Lozier, S., Marotzke, J., and Sutton, R.: Past, present, and future changes in the atlantic meridional overturning circulation, *B. Am. Meteorol. Soc.*, 93, 1663–1676, doi:10.1175/BAMS-D-11-00151.1, 2012. 1766, 1768, 1775
- Tapley, B. D., Bettadpur, S., Ries, J. C., Thompson, P. F., and Watkins, M. M.: GRACE Measurements of Mass Variability in the Earth System, *Science*, 305, 503–505, doi:10.1126/science.1099192, 2004. 1767, 1770
- Vellinga, M. and Wood, R. A.: Global Climatic Impacts of a Collapse of the Atlantic Thermohaline Circulation, *Clim. Change*, 54, 251–267, 2002. 1767
- Wahr, J., Molenaar, M., and Bryan, F.: Time variability of the Earth's gravity field: Hydrological and oceanic effects and their possible detection using GRACE, *J. Geophys. Res.*, 103, 205–229, doi:10.1029/98JB02844, 1998. 1772
- Watkins, M. M., Wiese, D. N., Yuan, D.-N., Boening, C., and Landerer, F. W.: Improved methods for observing Earth's time variable mass distribution with GRACE using spherical cap mascons, *J. Geophys. Res.-Sol. Ea.*, 120, 2648–2671, doi:10.1002/2014JB011547, 2015. 1771, 1772, 1775, 1783

Wunsch, C. and Heimbach, P.: Two decades of the atlantic meridional overturning circulation: Anatomy, variations, extremes, prediction, and overcoming its limitations, J. Clim., 26, 7167–7186, doi:10.1175/JCLI-D-12-00478.1, 2013. 1767, 1768

5 Zhang, R.: Coherent surface-subsurface fingerprint of the Atlantic meridional overturning circulation, Geophys. Res. Lett., 35, 1–6, doi:10.1029/2008GL035463, 2008. 1767

**Monitoring AMOC  
with GRACE**

K. Bentel et al.

Title Page

Abstract

Introduction

Conclusions

References

Tables

Figures



Back

Close

Full Screen / Esc

Printer-friendly Version

Interactive Discussion



Monitoring AMOC  
with GRACE

K. Bentel et al.

Title Page

Abstract

Introduction

Conclusions

References

Tables

Figures



Back

Close

Full Screen / Esc

Printer-friendly Version

Interactive Discussion

**Table 1.** Overview of the different resolutions of the synthetic OBP data.

Acronym	Characteristics	Spatial resolution
$T^O$	Original ECCO2 OBP grid	0.25°
$T^{SH60}$	Spherical harmonic expansion up to d/o 60, smoothed with a Gaussian filter of 300 km radius and synthesized back to a point grid	3°
$T^{MSC}$	Interpolated to approx. 3° equalarea JPL mascon grid, which is described in Watkins et al. (2015)	3°
$T^{MSC+CRI}$	Interpolated to approx. 3° equal area JPLmascon grid, and CRI (coastline resolution improvement) applied (Watkins et al., 2015)	3°
$T^{MSC+POSOPT}$	Interpolated to a grid similar to the JPL mascon grid, with the grid cells' longitude position adjusted to minimized RMS error (minimizing leakage over different depths and land hydrology leakage simultaneously)	3°

Monitoring AMOC  
with GRACE

K. Bentel et al.

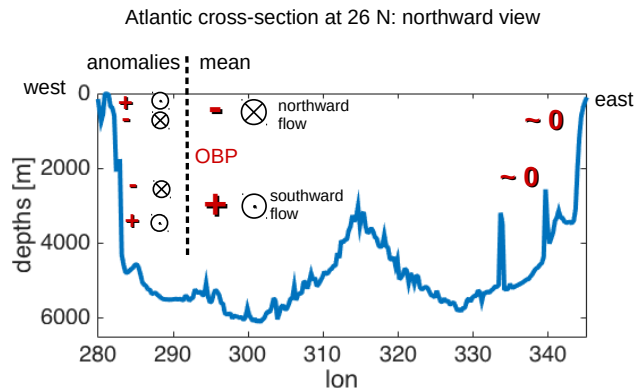


**Figure 1.** Cross-section of the North Atlantic with an illustration of north- and southward flow and associated ocean bottom pressure mean and anomalies along the basin boundaries. Note that in the actual ocean, the bottom pressure signals are largest along the Western boundary and the bottom pressure at the Eastern boundary is very small and can be neglected. Ocean bottom pressure anomalies are observable with satellite gravimetry

[Title Page](#)[Abstract](#)[Introduction](#)[Conclusions](#)[References](#)[Tables](#)[Figures](#)[◀](#)[▶](#)[◀](#)[▶](#)[Back](#)[Close](#)[Full Screen / Esc](#)[Printer-friendly Version](#)[Interactive Discussion](#)

**Monitoring AMOC  
with GRACE**

K. Bentel et al.

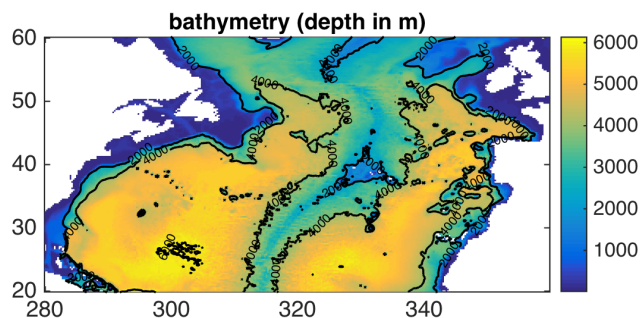


**Figure 2.** Bathymetry for the North Atlantic with the 2000, 4000, and 6000 m depth contour lines

Title Page

Abstract

Introduction

Conclusions

References

Tables

Figures

◀

▶

◀

▶

Back

Close

Full Screen / Esc

Printer-friendly Version

Interactive Discussion



## Monitoring AMOC with GRACE

K. Bentel et al.

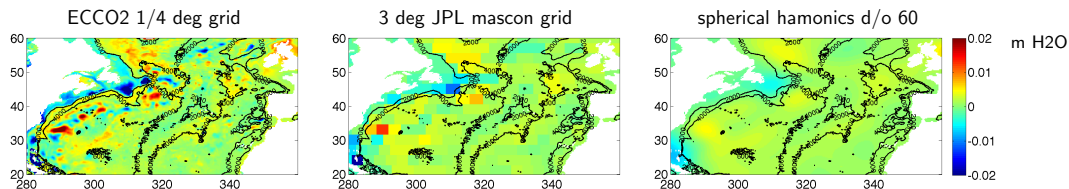


**Figure 3.** OBP snapshots for January 2012 for the different simulated OBP observation time series: left:  $0.25^\circ$  ECCO2 resolution; center: GRACE JPL mascon resolution (approx.  $3^\circ$ ); right: GRACE spherical harmonic resolution to sh degree 60, smoothed with a 300 km Gaussian filter

Title Page

Abstract

Introduction

Conclusions

References

Tables

Figures

◀

▶

◀

▶

Back

Close

Full Screen / Esc

Printer-friendly Version

Interactive Discussion



Monitoring AMOC  
with GRACE

K. Bentel et al.

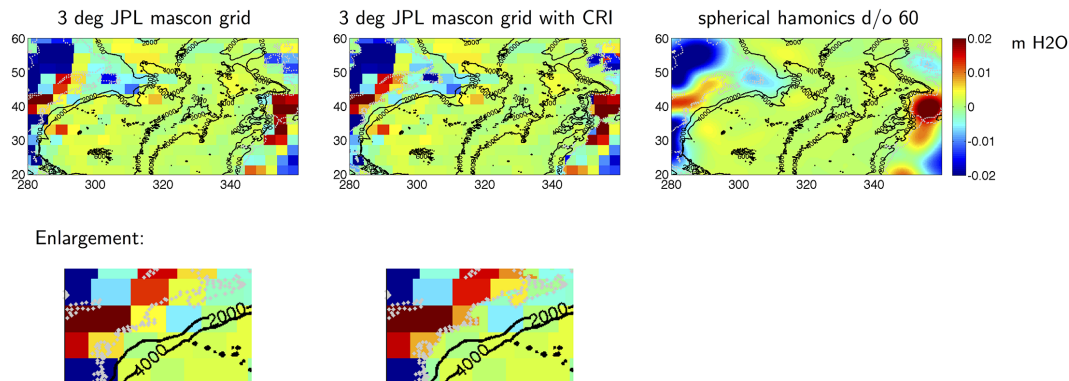


**Figure 4.** OBP snapshots for January 2012 for the simulated observations, including the continental hydrology signal: left: JPL mascon grid without CRI (coastline resolution improvement); center: JPL mascon grid with CRI, right: spherical harmonics to  $60^\circ$ . Since the ECCO2 original data is not smoothed, the OBP pixels do not get affected by nearby land hydrology signals (therefore no additional plot for hydrology). Second row shows enlargements of the two mascon-resolution data sets including hydrology and details for CRI

Title Page

Abstract

Introduction

Conclusions

References

Tables

Figures

◀

▶

◀

▶

Back

Close

Full Screen / Esc

Printer-friendly Version

Interactive Discussion



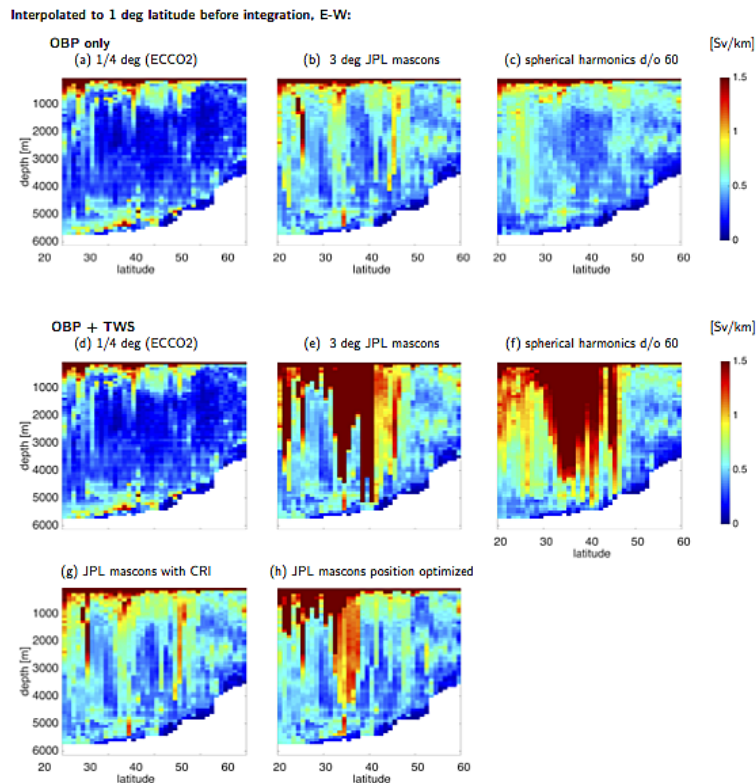


**Figure 5.** RMS errors for the computed transport  $T$  in  $[\text{Sv km}^{-1}]$  from Eastern and Western boundary OBP according to Eq. (3). OBP only (top row) and OBP + hydrology (second and third row) for each of the synthetic observation time series. Significant leakage errors are introduced with the GRACE-like resolutions (second row), CRI filtering of the mascons and optimizing their position in longitude can remove a major part of the leakage errors

**Monitoring AMOC  
with GRACE**

K. Bentel et al.

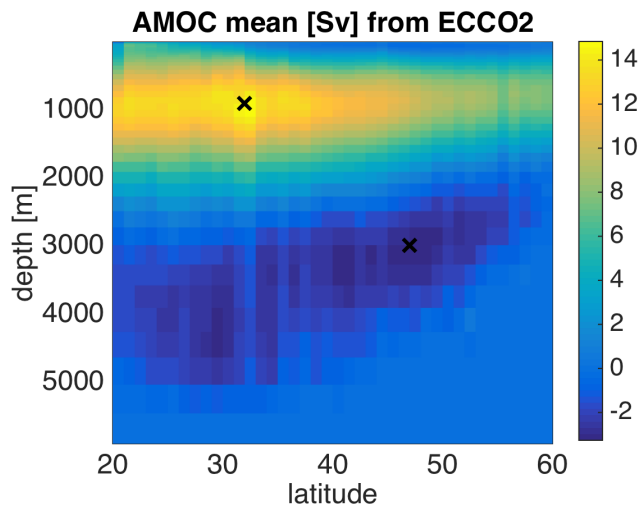


**Figure 6.** Time mean of AMOC from ECCO2, with maximum at 32° N, 909 m depth, minimum at 47° N, 2990 m depth, both indicated marker X.

[Title Page](#)[Abstract](#)[Introduction](#)[Conclusions](#)[References](#)[Tables](#)[Figures](#)[◀](#)[▶](#)[◀](#)[▶](#)[Back](#)[Close](#)[Full Screen / Esc](#)[Printer-friendly Version](#)[Interactive Discussion](#)

Monitoring AMOC  
with GRACE

K. Bentel et al.

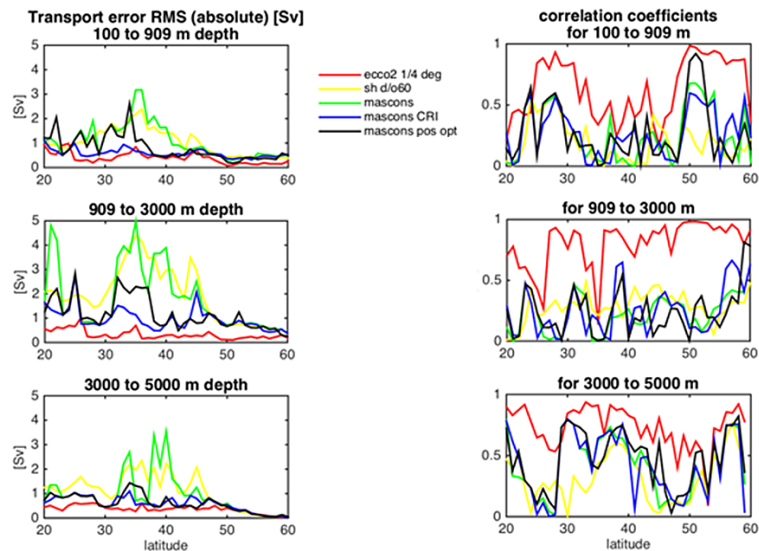


**Figure 7.** Error RMS and correlation coefficients for reconstructed net transport in three different depth layers and from different OPB resolutions (native ECCO2 grid vs. GRACE-like resolutions)



Back

Close

Full Screen / Esc

Printer-friendly Version

Interactive Discussion



**Monitoring AMOC with GRACE**

K. Bentel et al.

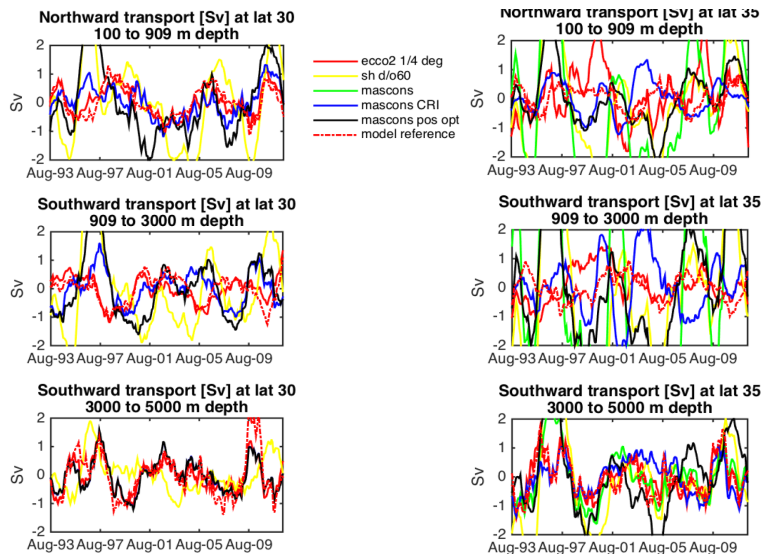


**Figure 8.** Transport time series at two specific latitudes; reconstruction from OBP versus model baseline (from velocities)

Title Page

Abstract Introduction

Conclusions References

Tables Figures

◀ ▶

◀ ▶

Back Close

Full Screen / Esc

Printer-friendly Version

Interactive Discussion

